6-2020

Passive Quadrupedal Gait Synchronization for Extra Robotic Legs Using a Dynamically Coupled Double Rimless Wheel Model

Daniel J. Gonzalez
USMA West Point & MIT, daniel.gonzalez@westpoint.edu

Harry Asada
MIT, asada@mit.edu

Passive Quadrupedal Gait Synchronization for Extra Robotic Legs Using a Dynamically Coupled Double Rimless Wheel Model

Daniel J. Gonzalez, *Member, IEEE*[1], and H. Harry Asada, *Member, IEEE*[2]

***Abstract*— The Extra Robotic Legs (XRL) system is a robotic augmentation worn by a human operator consisting of two articulated robot legs that walk with the operator and help bear a heavy backpack payload. It is desirable for the Human-XRL quadruped system to walk with the rear legs lead the front by 25% of the gait period, minimizing the energy lost from foot impacts while maximizing balance stability. Unlike quadrupedal robots, the XRL cannot command the human's limbs to coordinate quadrupedal locomotion. Connecting the XRL to the human using a passive coupler, we have found that the two bipeds converge to the desired phase difference without active control. Using a pair of Rimless Wheel models, it is shown that the systems coupled with a spring and damper converge to the desired 25% phase difference. A Poincaré return map was generated using numerical simulation to examine the convergence properties to different coupler design parameters, and initial conditions. The Dynamically Coupled Double Rimless Wheel system was physically realized with a spring and dashpot chosen from the theoretical results, and initial experiments indicate that the desired synchronization properties may be achieved within several steps using this set of passive components alone.**

Keywords: Human Augmentation, Supernumerary Robotic Limbs, Exoskeletons, Locomotion, Nonlinear Dynamics

I. Introduction and Motivation

The Extra Robotic Legs (XRL) system aims to empower the industrial worker and emergency responder to enhance their ability to perform their job by alleviating the burden of heavy equipment and enabling them to execute strenuous maneuvers more easily. The XRL system was designed to allow United States Department of Energy (DOE) nuclear decommissioning workers to carry more life support equipment (such as an air tank, extra tools, and a body cooling system) to increase their "stay time" at the task location, and to support workers in general who must take kneeling, crouching, and other fatiguing postures near the ground [1]. Previous work has explored the shared control of balance while the operator squats down to the ground [2]. We now investigate the synchronization of the human and XRL bipedal systems with each other during steady-state locomotion.

[1]D. J. Gonzalez is with both the Robotics Research Center in the Department of Electrical Engineering and Computer Science at the United States Military Academy, West Point, NY 10996, USA and the d'Arbeloff Laboratory for Information Systems and Technology in the Department of Mechanical Engineering, Massachusetts Institute of Technology, Cambridge, MA 02139, USA. Email: daniel.gonzalez@westpoint.edu and dgonz@mit.edu

[2]H. H. Asada is with the d'Arbeloff Laboratory for Information Systems and Technology in the Department of Mechanical Engineering, Massachusetts Institute of Technology, Cambridge, MA 02139, USA. Email: asada@mit.edu

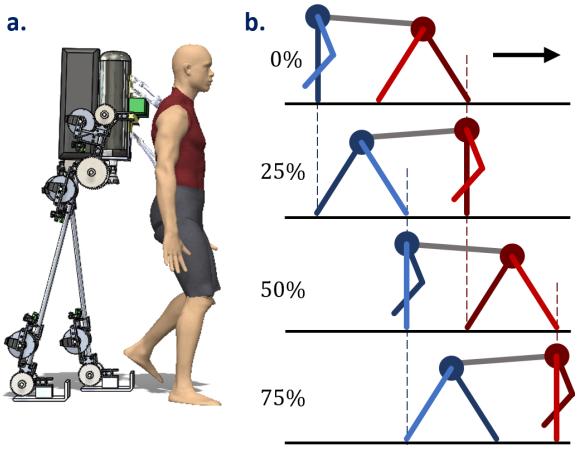

Fig. 1: The Extra Robotic Legs System and desired gait cycle, with the hind legs leading the rear legs by 25%. Note that this quadrupedal system behaves as if it were two coupled bipeds.

When walking together, the human-XRL system forms a type of quadrupedal system (See Fig. 1). Unlike fully biological or fully robotic quadrupeds, the human-XRL system consists of two independently controlled biped systems which are physically connected; one is a human and the other is a robot. The synchronization challenge arises from the fact that there is no centralized controller to command the entire quadruped. Rather, the human and robot bipedal systems are functionally independent. The human gait is not directly controllable from the robot side, but can be indirectly affected through the coupler that physically connects the two. Apart from adding sensors to the human for the robot to monitor, their interaction is purely physical. The XRL gait control must be designed by considering the unique properties of the system: a) the bidirectional nature of the dynamic interactions, and b) the limited sensing and control over the human gait through the physical coupling. Our goal is to establish a natural regulator that achieves a desired gait cycle by exploiting the intrinsic dynamic synchronization properties of the human-XRL system.

This desired gait cycle comes from studying animal biomechanics. Analysis of quadrupedal animal gaits [3] shows that quadrupeds behave as if they were two coupled bipeds and tend to fall into a gait cycle where the hind limbs lead the fore limbs by about 25% of the stride time (or 90° out of phase) during steady-state walking, as shown in Fig. 1. This walking gait cycle in which the footfalls are timed in

a 1-4-2-3 sequence (numbered clockwise starting from the front-left foot) has also been found to maximize the margin of stability of the quadruped's balance [4]. It has also been shown that gaits with more sequenced collisions per stride (such as in the four-beat walking gait) are more energy effective than gaits which group multiple foot collisions together [5]. Using a quadrupedal model incorporating legs with mass and a wobbling mass passively connected to a rigid body, the four-beat gait can be stabilized [6]. It is of interest, then, to analyze how intrinsic dynamics can lead the Human-XRL System to naturally fall into this special gait cycle.

We will show that this desirable gait can be achieved by simply connecting the two biped systems with the proper passive dynamic coupler. This is an interesting phenomenon, since we neither force the human to follow a desired gait pattern, nor actively control the XRL to track the desired gait. Intrinsic dynamics of the interacting biped systems bring the mutual gait to the desired one. The dynamic coupler, which is a passive device, contracts the two nonlinear dynamical systems towards a desired stable limit cycle.

It is imperative that the interactive nature of the dynamics between the human and the XRL be taken into account in analyzing and achieving synchronization, because the XRL is physically attached to the human. Motion from the XRL perturbs the human, and vice-versa through bidirectional interactions. Both the human and XRL must individually establish a steady gait cycle while experiencing interference from the other. The challenge is to assure that the two gaits can be coordinated properly despite, or perhaps because of, the bidirectional dynamic interaction. Passive quadrupedal synchronization has an application in not only the XRL system, but can also inform the mechanical and control design of more general quadrupedal robots.

In this work, we aim to establish an interactive passive gait synchronization method for the human-XRL system. In Section II we introduce and analyze a simple, yet novel, quadrupedal walking model consisting of two Rimless Wheel biped systems connected with a dynamic coupler: the Dynamically Coupled Double Rimless Wheel model. Property-agnostic coupler conditions that maximize the convergence rate are found using a numerically acquired Poincaré map in Section III. Synchronization is demonstrated on a physically realized Coupled Rimless Wheel pair in Section IV. Section V provides a conclusion and outlines future work to be conducted.

II. The Dynamically Coupled Double Rimless Wheel Model

The canonical Rimless Wheel model [7] is a simple model that captures natural bipedal walking dynamics. The Rimless Wheel model has been extended to capture quadrupedal walking dynamics by coupling a pair of Rimless Wheels with a rigid beam and forcing a set footfall timing sequence [8]. Stable walking limit cycles can be observed with this model, though the gait cycle phase is strictly enforced through kinematics. Such a system was then shown to maximize passive steady-state velocity when the phase parameter was chosen to be perfectly out of phase, or 50% out of phase[1] [9]. We now introduce some novel modifications of our own.

In order to explore the effects of dynamic coupling, we extend the Rimless Wheel model by adding a second Rimless Wheel and connecting the two with a passive coupler made up of a spring k and a viscous damper b in parallel.

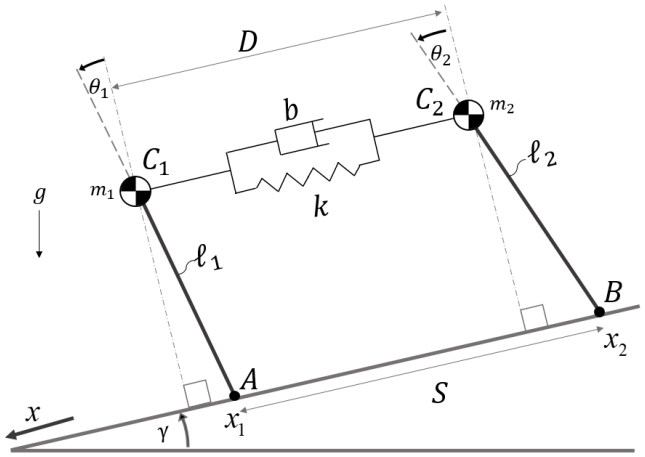

Fig. 2: The Coupled Rimless Wheels Model

Characteristic to our human-XRL system is that this coupler is dynamic rather than rigid. Smith and Berkmeier use a rigid connection, which kinematically couples the angles θ_1 and θ_2 and the angular velocities $\dot{\theta}_1$ and $\dot{\theta}_2$ [8]. Once a set of initial conditions has been chosen, the rigidly coupled Rimless Wheels cannot change their relative phase.

Our novel model, by including a passive spring and damper connecting the two wheels, allows the angles and angular velocities of each wheel to move independently, allowing for rich dynamic interactions between the two. Tuning design parameters k and b can affect the mutual dynamics and gait cycle. Indeed, it is through this mechanism that we aim to synchronize the gait cycle of the first and second Rimless Wheels.

The masses m_1 and m_2 of each pendulum are point masses atop massless links of length ℓ_1 and ℓ_2, respectively. The angle of the first Rimless Wheel about point A is θ_1 and the angle of the second about point B is θ_2, and the step angles for each are α_1 and α_2. The distance between the coupler endpoints is D and the unstretched length of the spring is D_0. See Fig. 2.

The force balance equations for the Rimless Wheels are

$$\begin{aligned} m_1\ell_1^2\ddot{\theta}_1 =& m_1 g\ell_1 \sin(\theta_1+\gamma) \\ & -F_c\ell_1(\cos\theta_1\cos\beta-\sin\theta_1\sin\beta) \end{aligned} \tag{1}$$

[1]Note that in quadrupedal locomotion we consider the system to be at our desired gait cycle when the hind legs are 25% out of phase with the front, but in planar models there is no distinction between the left or right legs, and thus we consider successful synchronization to be achieved when the stance leg of the front and rear halves are 50% out of phase from each other. The additional virtual pair of legs in the swing phase are not taken into account in this model.

$$
\begin{aligned}
m_2\ell_2^2\ddot{\theta}_2 =& m_2 g\ell_2 \sin(\theta_2+\gamma) \\
&+F_c\ell_2(\cos\theta_2\cos\beta-\sin\theta_2\sin\beta)
\end{aligned} \tag{2}
$$

where the coupler force is

$$
F_c = k(D-D_0)+b\dot{D} \tag{3}
$$

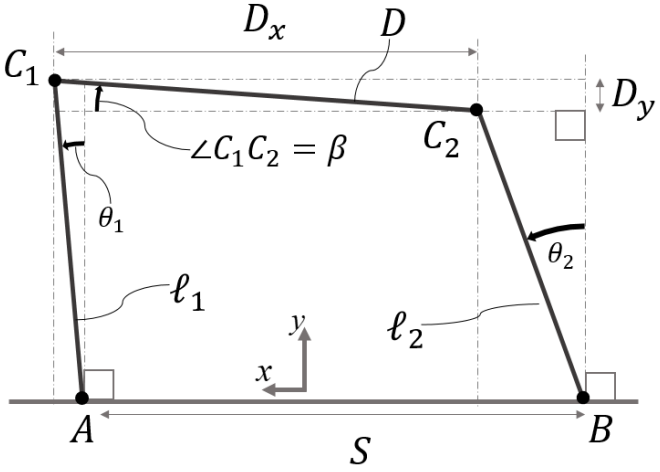

Fig. 3: Geometric Relationship for D and β.

The coupler of length D acts between the two pendula and has an orientation β relative to the sloped ground surface. See Fig. 3 for details. The x-component of D is

$$
D_x = D\cos\beta = \ell_1\sin\theta_1-\ell_2\sin\theta_2+S \tag{4}
$$

and the y-component of D is

$$
D_y = D\sin\beta = \ell_1\cos\theta_1-\ell_2\cos\theta_2 \tag{5}
$$

where S is the distance between the stance foot locations x_1 and x_2 of each Rimless Wheel i

$$
S = x_1-x_2 \tag{6}
$$

From these components, we find the coupler distance

$$
D = \sqrt{D_x^2+D_y^2} \tag{7}
$$

the coupler angle

$$
\beta = \sin^{-1}\left(\frac{\ell_1\cos\theta_1-\ell_2\cos\theta_2}{D}\right) \tag{8}
$$

and the coupler distance time derivative

$$
\dot{D} = \frac{D_x\dot{D}_x+D_y\dot{D}_y}{D} \tag{9}
$$

where

$$
\dot{D}_x = \ell_1\cos(\theta_1)\dot{\theta}_1-\ell_2\cos(\theta_2)\dot{\theta}_2 \tag{10}
$$

and

$$
\dot{D}_y = \ell_2\sin(\theta_2)\dot{\theta}_2-\ell_1\sin(\theta_1)\dot{\theta}_1 \tag{11}
$$

resulting in

$$
\dot{D} = \ell_1\cos(\theta_1+\beta)\dot{\theta}_1-\ell_2\cos(\theta_2+\beta)\dot{\theta}_2 \tag{12}
$$

The stance distance S is piecewise constant

$$
S = S_0+n_1\sigma_1-n_2\sigma_2 \tag{13}
$$

and depends on the initial step length S_0, the number of steps taken by each wheel n_i and the step length σ_i for each Rimless Wheel

$$
\sigma_i = 2\ell\sin\alpha_i,\ i\in 1,2 \tag{14}
$$

If step lengths are the same ($\sigma_1=\sigma_2=\sigma$) then

$$
S = S_0+n\sigma \tag{15}
$$

where

$$
n = n_1-n_2 \tag{16}
$$

is the relative difference in the number of steps between the front and back halves. During normal operation, n is 0 or 1.

The nonlinear state-determined equations during the continuous dynamics are, assuming $\ell_1=\ell_2=\ell$ and $m_1=m_2=m$:

$$
\begin{aligned}
\ddot{\theta}_1 =& \frac{g}{\ell}\sin(\theta_1+\gamma) \\
&-\frac{k}{m\ell}(D-D_0)\cos(\theta_1+\beta) \\
&-\frac{b}{m}\left(\cos(\theta_1+\beta)\dot{\theta}_1-\cos(\theta_2+\beta)\dot{\theta}_2\right)\cos(\theta_1+\beta)
\end{aligned} \tag{17}
$$

$$
\begin{aligned}
\ddot{\theta}_2 =& \frac{g}{\ell}\sin(\theta_2+\gamma) \\
&+\frac{k}{m\ell}(D-D_0)\cos(\theta_2+\beta) \\
&+\frac{b}{m}\left(\cos(\theta_1+\beta)\dot{\theta}_1-\cos(\theta_2+\beta)\dot{\theta}_2\right)\cos(\theta_2+\beta)
\end{aligned} \tag{18}
$$

$$
\dot{D} = \ell\left(\cos(\theta_1+\beta)\dot{\theta}_1-\cos(\theta_2+\beta)\dot{\theta}_2\right) \tag{19}
$$

where, for brevity, we write

$$
\beta = \sin^{-1}\left(\frac{\ell}{D}(\cos\theta_1-\cos\theta_2)\right) \tag{20}
$$

and the state of the system can be fully determined with the following state vector

$$
x = \begin{bmatrix}\theta_1 & \dot{\theta}_1 & \theta_2 & \dot{\theta}_2 & D\end{bmatrix}^T \tag{21}
$$

where each of the five energy storage elements in the system (kinetic energy of each pendulum, gravitational potential energy of each pendulum, and potential energy stored in the spring) is associated with its own state variable.

The hybrid heel strike/toe-off dynamics are treated independently for each pendulum system at the angle limit α of forward lean before the swing leg impacts and becomes the new stance leg. Energy is lost by conserving only angular momentum about the new stance leg. The discrete jumps for the hybrid dynamical system occur as follows (assuming near-steady-state rolling in the positive θ direction):

A. when $\theta_1\geq\alpha$:
The angle instantaneously changes: $\theta_{1+}=-\alpha$;
The angular velocity instantaneously changes: $\dot{\theta}_{1+}=\dot{\theta}_{1-}\cos(2\alpha)$;
The difference in steps between Rimless Wheels 1 and 2 increases: $n=1$.

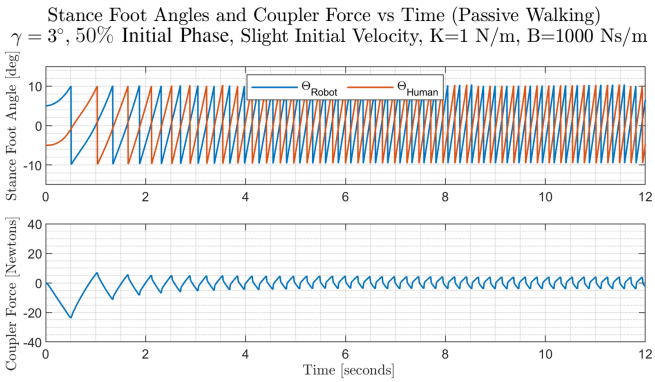

Fig. 4: Passive walk with desired 50% phase difference

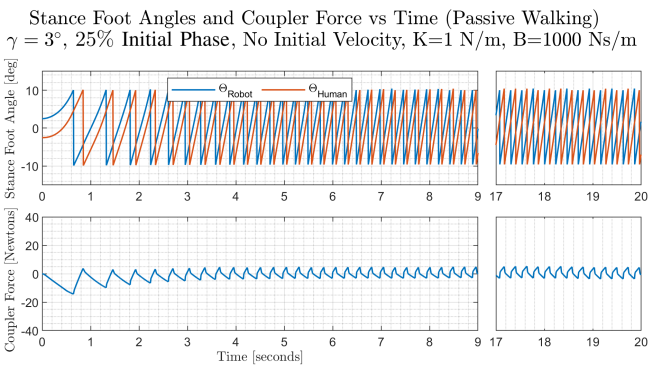

Fig. 5: Passive walk with initial phase difference of 25% converges to the desired 50% difference

B. when $\theta_2 \geq \alpha$:
The angle instantaneously changes: $\theta_{2+} = -\alpha$;
The angular velocity instantaneously changes: $\dot{\theta}_{2+} = \dot{\theta}_{2-} \cos(2\alpha)$;
The difference in steps between Rimless Wheels 1 and 2 decreases: $n = 0$.

Note that D is continuous and does not ever jump discretely, but $\dot{D}$ does abruptly jump due to its proportionality to $\dot{\theta}_1$ and $\dot{\theta}_2$.

A. Qualitative Properties of the Coupled Rimless Wheels Model from Simulation

Because the Coupled Rimless Wheels system has a straightforward state-space representation, it can be simulated using an ODE solver. The system, given a set of initial conditions, may be forward simulated an arbitrary amount of time. By simulating the system up to the Hybrid Dynamical switching trigger points (angles θ_1 or θ_2 reaching α), then resetting the initial conditions to meet the new case, the full Hybrid Dynamical system can be simulated continuously.

This simulation is used to introduce some interesting properties of the Coupled Rimless Wheels system and their implications on the overall Human-XRL walking system. For the following simulations assume that the first and second Rimless Wheels are physically identical ($\ell_1 = \ell_2 = \ell$ and $m_1 = m_2 = m$) and that a gentle incline angle $\gamma = 3°$, mass $m = 68$ kg (150 lbs), length $\ell = 1.5$ meters (60 inches), a step angle $2\alpha = 20°$, and $S_0 = D_0 = \ell/4$ were used as system parameters.

Fig. 4 shows the results of the system passively walking down a 3° slope. Note that the human gait and the robot gait are 50% out of phase for the total duration. Although the pace frequency increases, the phase difference remains at the desired 50%. The coupling force acting between the two generates a large restoring force initially. This was achieved with a relatively large damping coefficient, $B = 1 \times 10^3$ [Ns/m] and a smaller stiffness $K = 1 \times 10^0$ [N/m].

Fig. 5 shows the case where the initial phase difference between the human and the robot is 25% out of phase. As the human and robot walk down the slope, the phase difference shifts and converges to the desired 50%. If the two gaits are initially perfectly in-phase, i.e. 0%, no coupling force is generated and, therefore, the phase difference does not converge. It is an unstable equilibrium. However, if we apply a small disturbance by giving a small initial velocity to the system, it converges to the desired gait phase of 50%. Fig. 6 shows this convergence case. The two gaits are perfectly in phase in the beginning with only a small initial velocity difference. The rate of convergence is slow at first, but the phase difference converges to the desirable 50%. The coupling force brings the two bipedal systems to the desired quadrupedal gait.

When the two Rimless Wheels are disconnected, that is, when $k = 0$ and $b = 0$, each wheel walks independently. By using a dynamic coupler, we observe the above results, where the human and robot synchronize their cycles out of phase. This implies that the effect of coupling forces to drive the relative positions and velocities of the two Rimless Wheel systems closer together can naturally lead to a 50% out-of-phase gait cycle with the proper conditions and parameters.

If we design the robotic XRL system to stand and balance itself, take steps, and maintain stability when walking on its own, we can expect that connecting it to the human via the proper spring-dashpot will naturally lead the whole system to converge to the 25% out-of-phase 4-legged gait cycle. This makes sense physically because periodic motion of the human walking generates a force transmitted to the

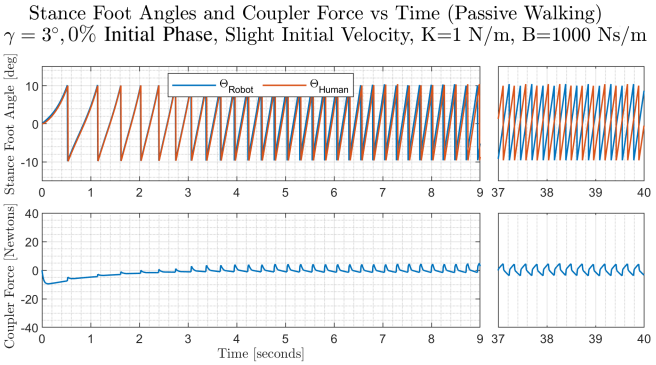

Fig. 6: Passive walk with initial phase difference of 0% and slight initial velocity converges to the desired 50% difference

robot with a phase shift. Because the magnitude of damping is higher than the magnitude of stiffness in this example, the generated coupler force is mostly proportional to the derivative of the displacement. Thus, the transmitted force to the robot is out of phase with of the resultant motion.

III. Coupler Parameters and Synchronization Rate

A. Nondimensionalized State Equations for the Coupled Rimless Wheels System

To generalize our numerical analysis of the properties of the Coupled Rimless Wheels System, we must first nondimensionalize the state equations.

Recall that the full nonlinear state equations are (17), (18), and (19). We first nondimensionalize the system by defining a unit time

$$\tau = t\sqrt{\ell/g} \tag{22}$$

which gives us the derivative conversion form

$$z'(\tau) = \frac{dz}{d\tau} = \frac{dz}{dt}\frac{dt}{d\tau} = \dot{z}(t)\sqrt{\frac{g}{\ell}}, \qquad z \in \theta_1, \theta_2, D \tag{23}$$

and the second derivative conversion form

$$z''(\tau) = \ddot{z}(t)\frac{g}{\ell}, \qquad z \in \theta_1, \theta_2, D \tag{24}$$

Finally, by choosing nondimensionalized parameters, initial conditions, and state variables

$$\hat{D} = \frac{D}{\ell},\ \hat{D_0} = \frac{D_0}{\ell},\ \hat{k} = \frac{k}{mg},\ \hat{b} = \frac{b}{m}\sqrt{\frac{\ell}{g}} \tag{25}$$

the nondimensionalized nonlinear state equations are

$$\begin{aligned}\theta_1'' =& \sin(\theta_1 + \gamma) \\ &-\hat{k}(\hat{D} - \hat{D}_0)\cos(\theta_1 + \beta) \\ &-\hat{b}\left(\cos(\theta_1 + \beta)\theta_1' - \cos(\theta_2 + \beta)\theta_2'\right)\cos(\theta_1 + \beta)\end{aligned} \tag{26}$$

$$\begin{aligned}\theta_2'' =& \sin(\theta_2 + \gamma) \\ &+\hat{k}(\hat{D} - \hat{D}_0)\cos(\theta_2 + \beta) \\ &+\hat{b}\left(\cos(\theta_1 + \beta)\theta_1' - \cos(\theta_2 + \beta)\theta_2'\right)\cos(\theta_2 + \beta)\end{aligned} \tag{27}$$

$$\hat{D}' = \cos(\theta_1 + \beta)\theta_1' - \cos(\theta_2 + \beta)\theta_2' \tag{28}$$

where for brevity we write

$$\beta = \sin^{-1}\left(\frac{\cos\theta_1 - \cos\theta_2}{\hat{D}}\right) \tag{29}$$

which have an augmented state vector

$$\hat{x} = \begin{bmatrix}\theta_1 & \theta_1' & \theta_2 & \theta_2' & \hat{D}\end{bmatrix}^T \tag{30}$$

and whose continuous dynamics are only dependent on the parameters γ, $\hat{D}_0$ $\hat{k}$, and $\hat{b}$ and hybrid switching dependent on α. The discrete jumps for the nondimensionalized hybrid dynamical system are identical to those in Section II.

B. Acquisition of Optimal Coupling Parameters via Numerical Poincaré Return Map

We now aim to find the stiffness k and damping b with the highest rate of convergence to synchronize a given system with a set of mass and length parameters. We will consider only the effects of $\hat{k}$ and $\hat{b}$ on the nondimensionalized system, which can then be used to find the physical stiffness k and damping b after scaling using physical parameters.

Due to our system's behavior as a stable limit cycle oscillator, we will analyze the convergence of θ_2 from one oscillation period to the next using a Poincaré return map. Consider a state-determined stable limit cycle oscillator with a state $x \in \Re^n$. There is a periodic orbit in the phase plane of this system. We define a Surface of Section (which can be an $n-1$ dimensional hyperplane transverse to the stable orbit at some specific point in the trajectory) through which intersect all trajectories converging to the stable limit cycle. If this hyperplane is orthonormal to one state variable in the phase plane, then the intersecting points are part of a reduced dimension Poincaré state vector $x_p \in \Re^{n-1}$. A stable fixed point of this discrete Poincaré system implies a stable limit cycle of the original system.

A Poincaré return map $P()$ is an autonomous function representing the reduced state after one orbit to timestep $k+1$ given the state at time k

$$x_p[k+1] = P(x_p[k]) \tag{31}$$

The Poincaré return map $P()$ can be linearized about an equilibrium as

$$x_p[k+1] = \frac{dP(x_p[k])}{dx_p}x_p[k] = Ax_p[k] \tag{32}$$

Because this is a discrete system, the eigenvalues λ_i of matrix A represent the dynamic response of the linearized system, which informs the local dynamic response of $P()$. If $|\lambda_i| < 1, \quad i \in [1 : n-1]$ then the discrete system is stable. The state x_p at time m given some initial condition $x_p[0]$ can be linearly approximated as

$$x_p[m] = A^m x_p[0] \tag{33}$$

For the Nondimensionalized Dynamically Coupled Double Rimless Wheel system, we have a continuous time state vector

$$x = \begin{bmatrix}\theta_1 & \theta_1' & \theta_2 & \theta_2' & \hat{D}\end{bmatrix}^T \tag{34}$$

We take a Surface of Section during the transition when $\theta_1 = \alpha$ and takes a step. We wish for θ_2 to converge to 0° along this Surface of Section. Our augmented state vector is now

$$x_p = \begin{bmatrix}\theta_1' & \theta_2 & \theta_2' & \hat{D}\end{bmatrix}^T \tag{35}$$

The analytical solution to the time response of (17), (18), and (19) is dependent on knowing the time spent in both cases of continuous motion, which we do not know a priori. Thus, the analytical Poincaré return map for the Coupled Rimless Wheels system can be intractable to solve for, but the linear matrix A may be obtained numerically using data collected from several simulated trajectories.

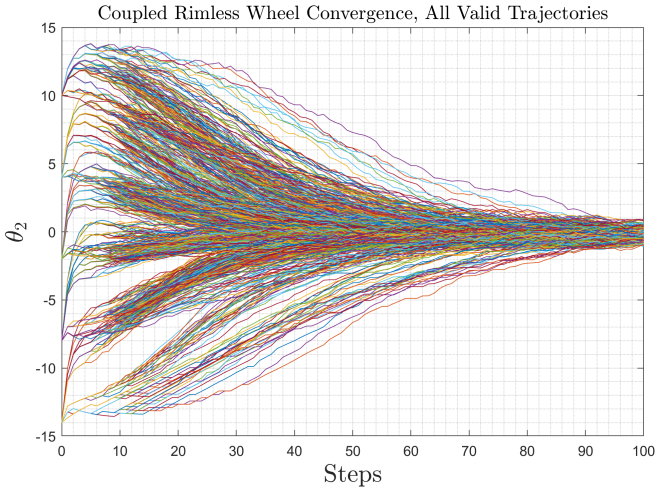

Fig. 7: All converging trajectories from the set of numerical simulations.

Consider a trajectory of x_p from an initial condition $x_p[0]$ to some convergent value $x_p[M]$ after M discrete samples. Now we run K different trials of the same system at different initial conditions, for a total of $M \times K$ samples of x. These data may be used to formulate an A matrix using Least Squares Regression, as adapted from Chapter 3 of [10].

We wish to find matrix A that minimizes the squared error between our predicted value of $x_{pred}[k+1] = Ax[k]$ and the actual value $x[k+1]$. We may formulate this as an optimization:

$$J = \frac{1}{2}\sum_{k=1}^{K}\sum_{m=1}^{M-1}(Ax_p[m]-x_p[m+1])^T(Ax_p[m]-x_p[m+1]) \tag{36}$$

Taking the derivative and setting it equal to a zero matrix

$$\frac{dJ}{dA} = 0 = \sum_{k=1}^{K}\sum_{m=1}^{M-1}(Ax_p[m] - x_p[m+1])x_p^T[m] \tag{37}$$

we can distribute and rearrange (with the sums written in shorthand for brevity)

$$A\sum\sum x_p[m]x_p^T[m] = \sum\sum x_p[m+1]x_p^T[m] \tag{38}$$

Defining

$$P^{-1} = \sum_{k=1}^{K}\sum_{m=1}^{M-1} x_p[m]x_p^T[m] \tag{39}$$

and

$$B = \sum_{k=1}^{K}\sum_{m=1}^{M-1} x_p[m+1]x_p^T[m] \tag{40}$$

we obtain the final matrix

$$A = BP \tag{41}$$

The eigenvalues of A provide the system rate of convergence. By performing this operation for different system parameters and comparing the eigenvalues, the parameters that lead to the fastest convergence rate may be selected.

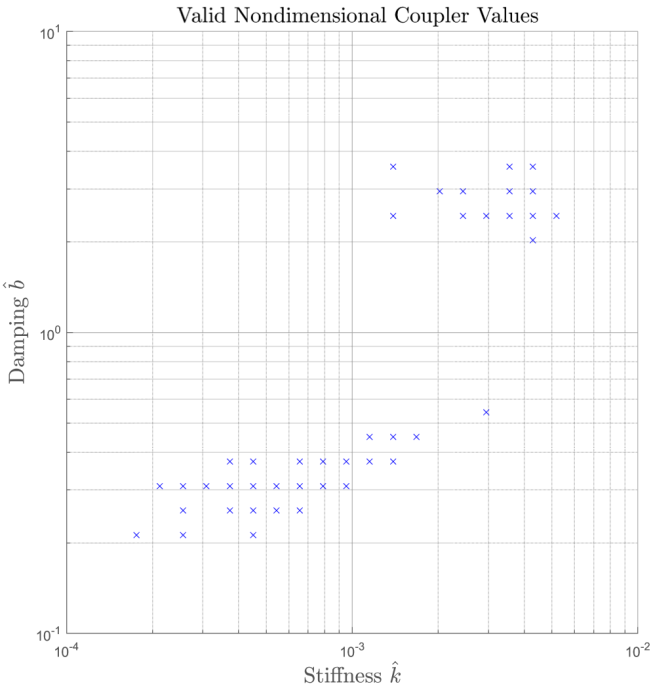

Fig. 8: Valid combinations of $\hat{k}$ and $\hat{b}$ which lead to converging systems.

Data were obtained via physics simulations that were run for systems with a slope angle $\gamma = 1.75°$ nondimensional stiffness $\hat{k}$ from 10^{-4} to 10^{-2} and damping $\hat{b}$ from 10^{-1} to 10^{1}. (Again, note that these parameters are nondimensional, but can be related to physical parameters using (25).) The same sets of initial conditions were used to generate the set of trajectories for each $[\hat{k}, \hat{b}]$ pair. From these sets of trajectories, the valid $[\hat{k}, \hat{b}]$ pairs were chosen. We consider valid combinations of $\hat{k}$ and $\hat{b}$ to be ones in which for all trajectories for all initial conditions $|\theta_2| < 1°$ within the simulation time. See Fig. 7 and Fig. 8. Note that two separate regions of continuous points exist, which may be the result of our time cutoff. While there may be additional stable parameter sets that only converge given significantly more time, these points are by definition not operationally useful for our application.

An A matrix was generated from each valid set of trajectory data corresponding to a valid $[\hat{k}, \hat{b}]$ pair. The dominant (largest magnitude) eigenvalue of each A was plotted for each $[\hat{k}, \hat{b}]$ pair in Fig. 9.

The $[\hat{k}, \hat{b}]$ pair having the lowest magnitude discrete eigenvalue was selected. The simulation trajectories and the Least Squares estimate of the trajectories for this best parameter set are shown in Fig. 10

IV. Experimental Validation of Passive Coupled Rimless Wheel Convergence to Gait Synchronization

A prototype Coupled Rimless Wheels system was built in order to test gait cycle convergence between two passive dynamic walkers (See Fig. 11). Each wheel was designed to

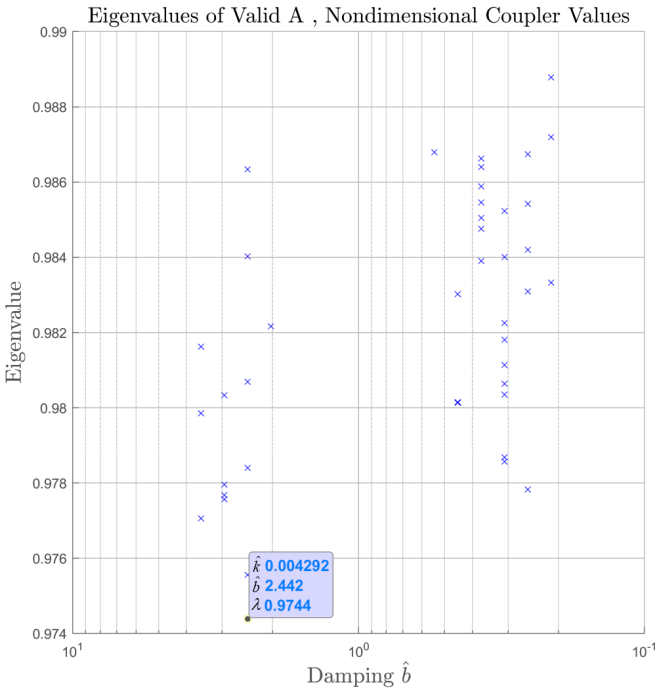

Fig. 9: Dominant eigenvalues of the linear Poincaré maps for converging systems for various nondimensional damping $\hat{b}$. Note that because these are discrete systems, 1 is the threshold for stability, and the farther from 1 the eigenvalue is, the faster the response.

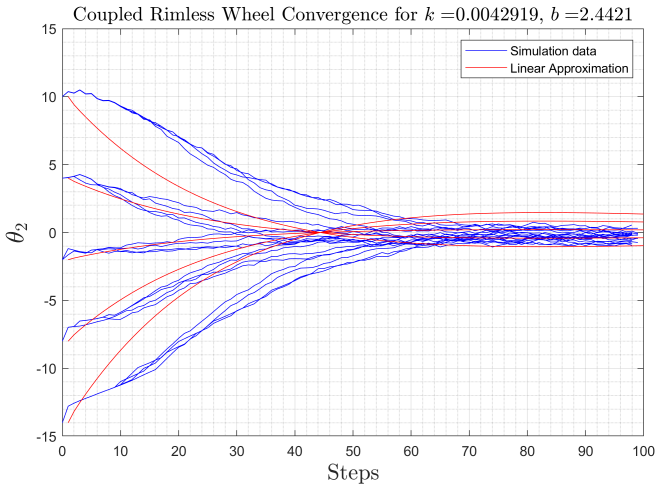

Fig. 10: Converging trajectory for the best stiffness and damping selected from the set of numerical simulations.

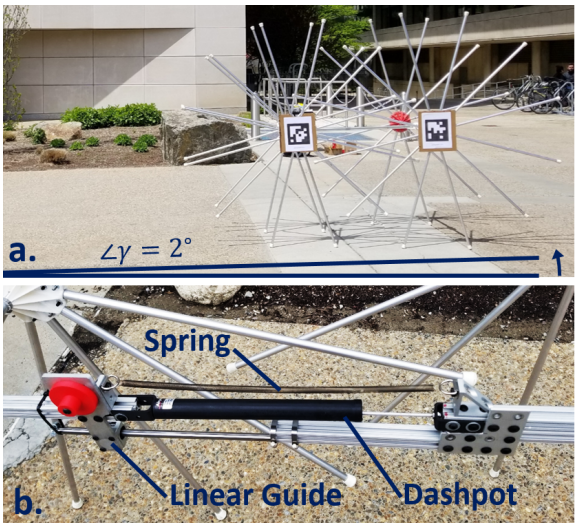

Fig. 11: Setup for testing synchronization of the Coupled Rimless Wheels system using a hardware-implemented spring-dashpot coupler.

be human-sized with $\ell = 0.9652$ meters (38 inches) which is the center of mass for a 1.7272 meter (5 foot 8 inch) tall male. Twelve spokes give each wheel a step angle $\alpha = 15°$.

Each Rimless Wheel consists of an identical pair of wheels, each with a hub made from ABS plastic, 12 spokes made of aluminum with rubber caps at the end of each for ground contact, and a rigid shaft, also aluminum, about which the coupler is free to rotate via a bearing. In order to track the position and orientation of each Rimless Wheel, AprilTag markers were mounted to the side of each wheel [11].

The coupler consists of a spring and a dashpot constrained to be loaded only linearly. A custom dashpot was made by the Airpot Corporation with a 280mm (11 inch) stroke and a hand-adjustable damping range from 0 [Ns/m] to 5234 [Ns/m]. The damper was tuned to be roughly 100 [Ns/m]. In order to overcome static friction in the dashpot, and due to the lack of practical availability of springs of lower stiffness, the coupler spring was chosen to be 5.25 [N/m]. See Fig. 11 for details.

The Coupled Rimless Wheels were sent down a gentle slope of $\gamma = 2°$ while a camera on a tripod filmed the result from the left side. Fig. 12 shows snapshots of the wheel's progress down the slope. The wheel phase converges to oscillate within $\pm 6\%$ of the desired phase difference of 50% from an initial condition of 21.6% within 7 steps. The difference in number of convergence steps between the simulation in Fig. 10 and the physical system can be attributed to a different slope angle γ and unmodeled dynamics such as elasticity in ground collisions and friction in the coupler bearing.

Fig. 13 shows the trajectory of the Rimless Wheels and the normalized angle difference

$$\phi = \theta_1 - \theta_2 \tag{42}$$

for the first 5 seconds of Trial 1. While ϕ is oscillatory, it converges to within $\pm 2°$ of the desired angle difference of $15°$ within several steps.

Fig. 14 shows the trajectory of the Rimless Wheels and the normalized angle difference ϕ for the first 5 seconds of Trial 2 (when both AprilTags were visible, as demonstrated in the supplementary video). Again, ϕ converges to within $\pm 2°$ of the desired angle difference of $15°$ within several steps.

These results validate the convergence of two coupled walking systems through passive means alone.

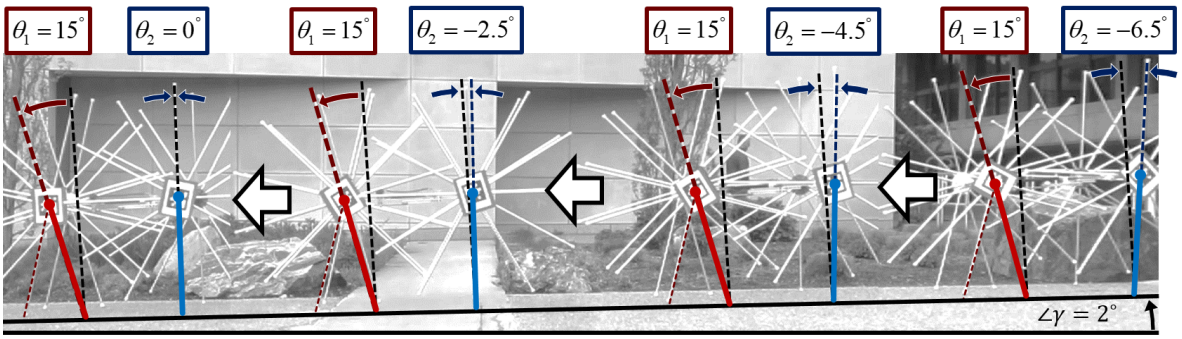

Fig. 12: Synchronization of a physically implemented Coupled Rimless Wheels system. The system synchronizes to the desired gait cycle within 7 steps.

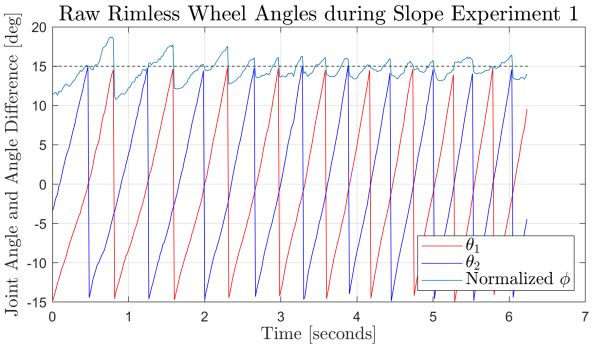

Fig. 13: θ_1, θ_2, and ϕ during Experiment Trial 1

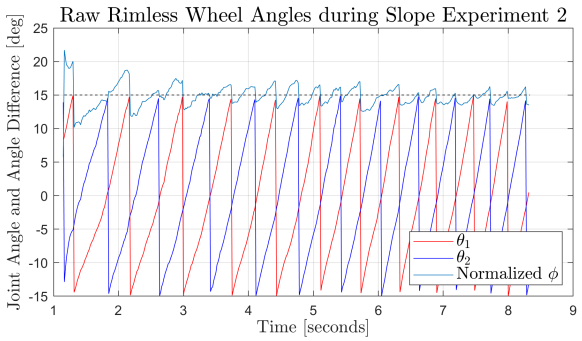

Fig. 14: θ_1, θ_2, and ϕ during Experiment Trial 2

V. Conclusion and Recommendations for Future Work

This work explored the use of a passive spring-dashpot to couple two hybrid dynamic limit cycle oscillators and synchronize their motion, with an application in coordinating the gait of the human-XRL quadrupedal system during steady state locomotion. A novel Dynamically Coupled Double Rimless Wheel model was formulated to capture these dynamic interactions, and it was shown that the system converges to a desired gait cycle for certain coupler parameters. A Poincarè map was numerically acquired and used to identify the coupler parameters leading to the fastest synchronization convergence. A physical pair of Rimless Wheel walkers was built and coupled with a spring-dashpot matching these parameter values. Synchronization was observed when this physical system walked down a gentle slope.

This truly passive method using a dynamic coupler is rather limited in flexibility and adaptability. To extend the utility, active control will be considered. This active control will be built on the basis of the intrinsically contracting dual biped systems. Rather than fighting against the intrinsic dynamics, it will exploit the natural properties of the system. Additional analysis of necessary and sufficient conditions for synchronized steady-state walking will be performed, as well as thorough experimentation to further validate our findings.

References

[1] D. J. Gonzalez and H. H. Asada, "Design of Extra Robotic Legs for Augmenting Human Payload Capabilities by Exploiting Singularity and Torque Redistribution," *IEEE International Conference on Intelligent Robots and Systems (IROS)*, 2018.

[2] D. J. Gonzalez and H. H. Asada, "Hybrid Open-Loop Closed-Loop Control of Coupled Human-Robot Balance During Assisted Stance Transition with Extra Robotic Legs," *IEEE Robotics and Automation Letters*, vol. 4, no. 2, pp. 1–1, 2019.

[3] T. M. Griffin, R. P. Main, and C. T. Farley, "Biomechanics of quadrupedal walking: how do four-legged animals achieve inverted pendulum-like movements?" *Journal of Experimental Biology*, vol. 207, no. 20, pp. 3545 LP – 3558, sep 2004. [Online]. Available: http://jeb.biologists.org/content/207/20/3545.abstract

[4] R. B. McGhee and A. A. Frank, "On the stability properties of quadruped creeping gaits," *Mathematical Biosciences*, vol. 3, no. 1-2, pp. 331–351, aug 1968. [Online]. Available: https://www.sciencedirect.com/science/article/pii/0025556468900904

[5] A. Ruina, J. E. Bertram, and M. Srinivasan, "A collisional model of the energetic cost of support work qualitatively explains leg sequencing in walking and galloping, pseudo-elastic leg behavior in running and the walk-to-run transition," *Journal of Theoretical Biology*, vol. 237, no. 2, pp. 170–192, 2005.

[6] C. D. Remy, K. Buffinton, and R. Siegwart, "Stability analysis of passive dynamic walking of quadrupeds," *International Journal of Robotics Research*, vol. 29, no. 9, pp. 1173–1185, 2010.

[7] T. McGeer, "Passive dynamic walking," *Intl. J. Robotics Research*, vol. 9, no. 2, pp. 62–82, 1990.

[8] A. Smith and M. Berkemeier, "Passive dynamic quadrupedal walking," in *International Conference on Robotics and Automation*, no. April, 1997, pp. 34–39.

[9] R. Inoue, F. Asano, D. Tanaka, and I. Tokuda, "Passive dynamic walking of combined rimless wheel and its speeding-up by adjustment of phase difference," *IEEE International Conference on Intelligent Robots and Systems*, vol. 3, no. 3, pp. 2747–2752, 2011.

[10] G. C. Goodwin and K. S. Sin, *Adaptive Filtering Prediction and Control*. New York, NY, USA: Dover Publications, Inc., 2009.

[11] E. Olson, "AprilTag: A robust and flexible visual fiducial system," in *IEEE International Conference on Robotics and Automation (ICRA)*, 2011.